FEKO-Based Method for Electromagnetic Simulation of Carcass Wires Embedded in Vehicle Tires

Nguyen Quoc Dinh[1], Takashi Teranishi[1], Naobumi Michishita[1], Yoshihide Yamada[1], and Koji Nakatani[2]

[1] Department of Electrical and Electronic Engineering, National Defense Academy
1-10-20 Hashirimizu, Yokosuka, Kanagawa 239-8686, Japan
g47098@nda.ac.jp, naobumi@nda.ac.jp, yyamada@nda.ac.jp

[2] The Yokohama Rubber Co., Ltd.
2-1 Oiwake, Hiratsuka, Kanagawa 254-8601, Japan
k.nakatani@mta.yrc.co.jp

Abstract ─ In a tire pressure monitoring system in which a pressure censor and a transmit antenna are contained in a tire, electromagnetic simulations of radiations from carcass embedded tires are requested. However, it is difficult to accurately determine these shielding effects.

In this study, methods for performing accurate electromagnetic simulation by adopting the MoM scheme are determined. In the study of the electric fields inside a tire, calculated results are compared with the theoretical distributions in a coaxial cylindrical resonator. In the case of a dense carcass arrangement, simulation results are in good agreement with theoretical results. In the study of electric fields penetrating carcass wires, the results of the MoM scheme are compared with those obtained using the finite element method (FEM). The adequate mesh size of the tire rubber in the MoM scheme for which the accuracy of the simulation results is guaranteed is established. Finally, electromagnetic simulations of an actual carcass tire model are performed.

Index Terms ─ Carcass tire, method of moment, normal-mode helical antenna, tire pressure monitoring system, tire rubber.

I. INTRODUCTION

In order to ensure safety in cars, tire pressure monitoring systems (TPMSs) have been introduced in the USA and Europe [1]. In Japan, the AIRwatch system for passenger cars has been developed [2, 3] by The Yokohama Rubber Co., Ltd. However, in the case of large vehicles, tires are reinforced by carcass wires. In such cases, the transmission of radio waves becomes very difficult. Therefore, a small normal-mode helical antenna (NMHA) that has a high antenna gain was developed [4]. In order to develop an efficient TPMS for carcass tires, the electric field distributions inside the tire and the radiation characteristics need to be determined by performing electromagnetic simulation. However, the structure of a tire rubber with densely embedded carcass wires is difficult to simulate in method of moment (MoM) simulations. Although, the NECBSC code seems effective [5], authors selected the FEKO simulator because of the excellent ability of simulations for large scale objects.

In this study, the accuracy of the simulation of the effects of carcass wires in tire rubber is determined by comparing simulation results with exact values. In section II, an outline of the TPMS, a simulation model of a carcass tire, and the electric characteristics of the NMHA are summarized. In section III, the accuracies of the simulation of the shielding effects of carcass wires are discussed by adopting the theoretical electric fields in a coaxial cylindrical resonator as an exact reference. In section IV, the accuracies of MoM simulations of the effects of tire rubber on electric field distributions are discussed by comparing MoM results with the accurate results obtained by using the finite element method (FEM). In section V, simulation results for an actual carcass tire model are shown. The computational costs of simulation, electric field

distributions around a tire, and radiation characteristics from a tire are presented.

II. OBJECTIVE SYSTEM AND SIMULATION MODEL

The AIRwatch system is illustrated in Fig. 1 [3]. Transmitters connected to tire pressure sensors are mounted on the wheels. A receiver unit is placed on the dashboard. A receiving antenna (film antenna) is attached to the windshield. Each of the sensors modulates continuous waves of 315 MHz with air pressure data using a frequency shift keying (FSK) scheme. The modulated waves are radiated from a transmit antenna in the sensor. The receiving antenna collects all the transmitted waves. The pressure levels are indicated on the receiver unit.

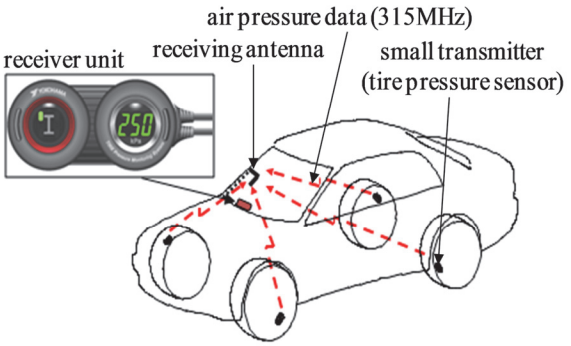

Fig. 1. The AIRwatch system.

The structure of the carcass tire to be analyzed and the position of the antenna in the tire are shown in Fig. 2. In an actual tire, a dense-mesh reinforcing structure called a tire belt is embedded in the tread of the tire. In the simulation, the model has a thin metal plate instead. Moreover, tires of large-sized vehicles are equipped with thin wires, called carcass, to reinforce the radial directions. The antenna inside the tire is almost enclosed by metal structures. The area within the broken lines corresponds to the tire model of Fig. 11, which is used to study the rubber effects.

Figure 3 shows the NMHA, which is used as the transmitting antenna [4]. This antenna is well known for having an electric current source (I) and a magnetic current source (J), as indicated in the figure. The magnetic current source achieves efficient radiations in a metal proximity use. Radiated electric field components from the magnetic and electric current sources are indicated by E_J and E_I, respectively. In order to contain this antenna inside a transmitter box, antenna size of 12.5 mm (0.01 wavelengths) diameter is determined. Since the input impedance becomes very small, a tap structure has been added to the NMHA in order to achieve impedance matching at 50 Ω.

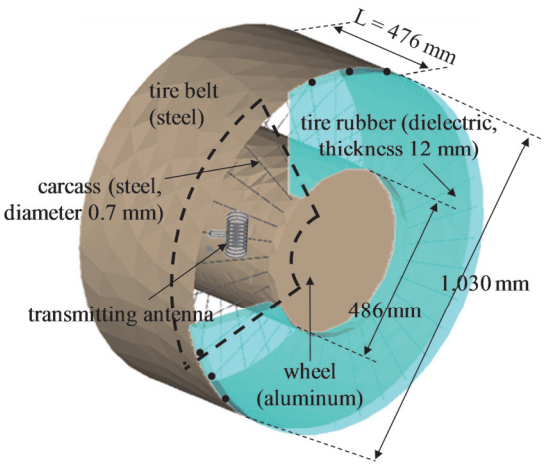

Fig. 2. Structure of a carcass tire.

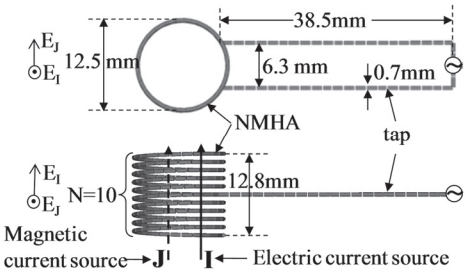

Fig. 3. Structure of a NMHA.

Radiation characteristics of the NMHA on a small metal plate are shown in Fig. 4. The tap is positioned opposite the metal plate. The E_J component becomes dominant. Antenna gain of -12.3 dBd (relative value to the half wave length dipole antenna) is achieved. A rather high antenna efficiency is achieved.

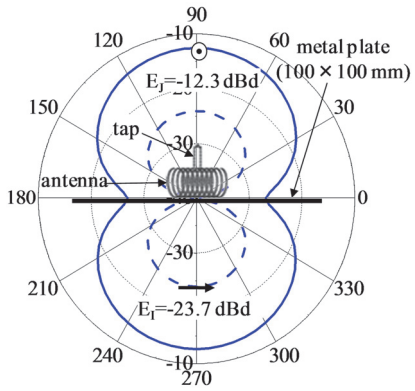

Fig. 4. Radiation characteristics of a NMHA.

III. SHIELDING EFFECTS BY CARCASS WIRES

A. Electric fields inside a tire

By taking into account the tire structure of Fig. 2, electric fields inside a tire are determined by metallic boundary conditions of a tire belt, wheel, and carcass [6]. Moreover, the tire rubber will affect the field distributions. In this section, affects of carcass are mainly investigated as the first step. Therefore, the rubbers are removed in the calculations. In order to evaluate the accuracy of the determined effects of carcass wires, the electric fields inside the tire were compared with that of a coaxial cylindrical resonator of a similar size to the tire. The structure shown in Fig. 2 is employed as the tire model in the simulation. The MoM code of FEKO is used. The structure of the cylindrical resonator is shown in Fig. 5. The outer and inner cylinders and the two side plates are all made of metals. In the sizes of actual tires, electric fields characterized by TEM and TE_{111} modes are dominant inside the coaxial cylinders. In particular, the TEM mode is the simplest because it only has radial electric field vectors. On the other hand, the TE_{111} mode has complex electric field vectors of radial and circumferential components. To determine if the simulation is adequate, it is appropriate to use the TEM mode. The resonance frequency of the TEM mode is given by the following equation.

$$L = s\lambda_0 / 2, \qquad (1)$$

where s is the mode variable. When s = 1, L = 475.8 mm gives a resonance frequency of 315 MHz.

A detailed view of the theoretical electric field distributions in the TEM mode is shown in Fig. 6. Here, R_1 = 515.0 mm and R_2 = 242.8 mm were used. In Fig. 6(a), all the electric field vectors are directed toward the radial directions. In Fig. 6(b), the electric fields vanish at the side plates. The electric field distributions inside the carcass tire are shown in Figs. 7 and 8. Figures 7 and 8 correspond to 288 and 36 carcass wires, respectively. In Fig. 7(a), the electric field vectors agree well with those in Fig. 6(a). In Fig. 7(b), the electric fields are confined to the inside of the tire. As for field intensities indicated beside the tire, electric fields on carcass wires become almost zero. This distribution agrees well with that in Fig. 6(b). Therefore, in this carcass number, carcass wires function like a complete shielding wall, which is the same as the side plate in Fig. 6.

In Fig. 8(a), deformations of the electric field vectors are observed. In Fig. 8(b), expansion of the electric fields outside the tire is observed. In electric field intensities indicated beside the tire, intensities on the carcass wire do not vanish. Electrical field distributions in the case of sparse carcasses seem reasonable.

In conclusion, the simulation results inside the carcass tire are considered adequate.

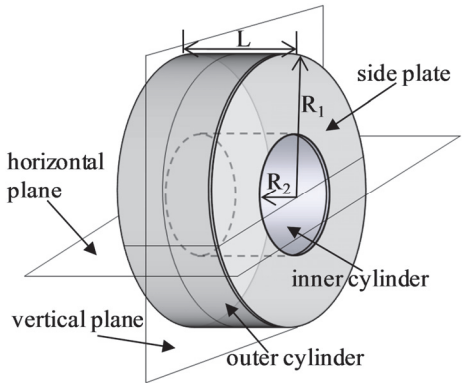

Fig. 5. Structure of a coaxial cylindrical resonator.

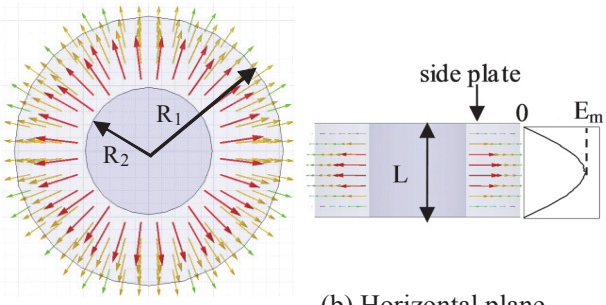

(a) Vertical plane. (b) Horizontal plane.

Fig. 6. Theoretical electric field distributions in the TEM mode.

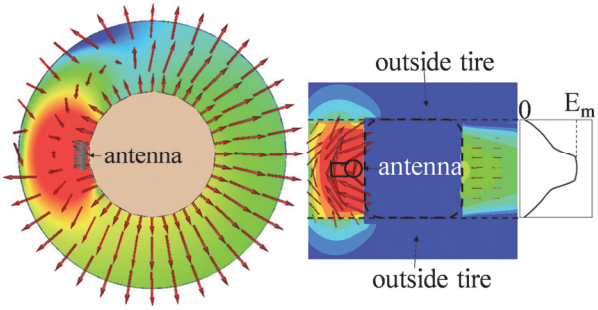

(a) Vertical plane. (b) Horizontal plane.

Fig. 7. Electric field distributions inside the tire (carcass wires: 288).

B. Radiation from a tire

The tire rubber is excluded from the structure shown in Fig. 2, and this structure is employed as the tire model in the simulation [6]. The MoM

code of FEKO is used. Radiation characteristics from a tire are shown in Fig. 9. In Fig. 9(a), a tire without carcass is shown. The electric fields in the TEM mode radiate through the apertures of the tire. The main beams exist in the direction of the Y axis. The maximum power becomes -4.2 dBd. In the direction of the X axis, a fairly strong beam is observed. Figure 9(b) shows a case where the number of carcass wires is 288. The main beam decreases by 32.5 dB. Figure 9(c) shows a case where the number of carcass wires is 36. The main beam decreases by 14.4 dB. Because the main beams in Figs. 9 (a), (b), and (c) are directed toward the Y axis, the powers at the receiving antenna, as depicted in Fig. 1, will deviate in accordance with the tire rotation. Actually, the severe fading caused by surrounding reflections is taken into account in the system design. The level deviation based on tire rotations will be taken into account as one of the fading factors. Antenna input impedances in the case of Fig. 9 are shown in Fig. 10. It is clarified that input impedances are not influenced by the presence of carcass wires.

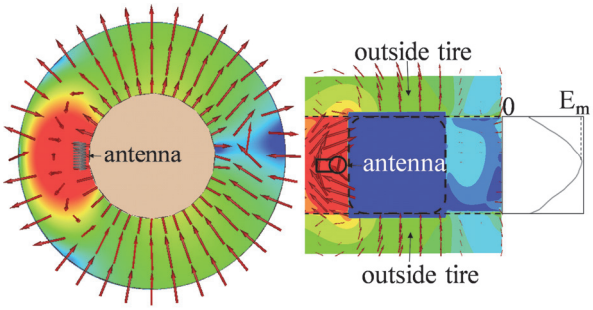

(a) Vertical plane. (b) Horizontal plane.

Fig. 8. Electric field distributions inside the tire (carcass wires: 36).

IV. SIMULATION METHOD OF A DIELECTRIC PLATE WITH EMBEDDED CARCASS WIRES

As for the structure of a dielectric plate with carcass wires inside, there were no study examples in FEKO simulation. Therefore, it is very important to ensure that the simulation is accurate. In order to investigate the fundamental effect of rubber, the effect on the electric field penetrations through carcass wires are considered. When the model shown in Fig. 2 is used in the calculation, the calculation load is very high. The simplified model shown in Fig. 11 that corresponds to the area within the broken lines in Fig. 2 is constructed. As for the radiator, a very small dipole antenna placed inside tire is employed for ease of calculation. This antenna is oriented in order to produce the E_J field component of Fig. 4 (parallel to the carcass wire). In accordance with the parallel electric field vectors, carcass wires are arranged in parallel wires of separations s. The observation planes are set perpendicular to the carcass wires. In order to eliminate the effects of edge currents, rather large values were selected for the sizes of the tire belt and wheel.

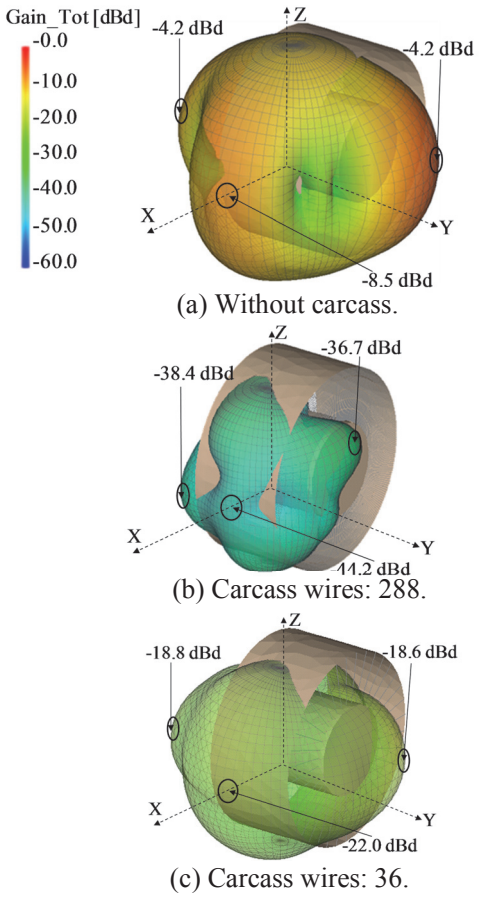

(a) Without carcass.

(b) Carcass wires: 288.

(c) Carcass wires: 36.

Fig. 9. Radiation characteristics from a tire (without rubber).

To assess the adequacy of the calculations, results obtained with MoM are compared with those obtained via FEM. Usually, the FEM results were considered to be the correct results. Comparisons of results are summarized in Table 1.

Firstly, the shielding effects of carcass wires are clearly shown by the HFSS simulation results. In the case where rubber was removed, electric fields passing through spaces between the wires gradually fade toward the outside. This result agrees very well with the physical behavior of parallel wires. Therefore, the HFSS result can be

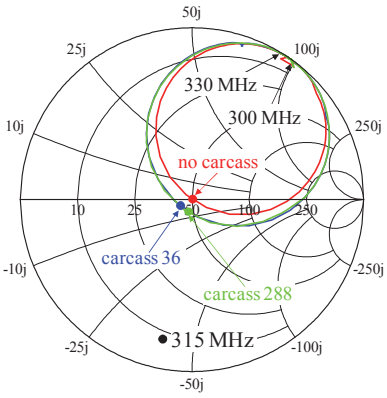

Fig. 10. Input impedance of the NMHA.

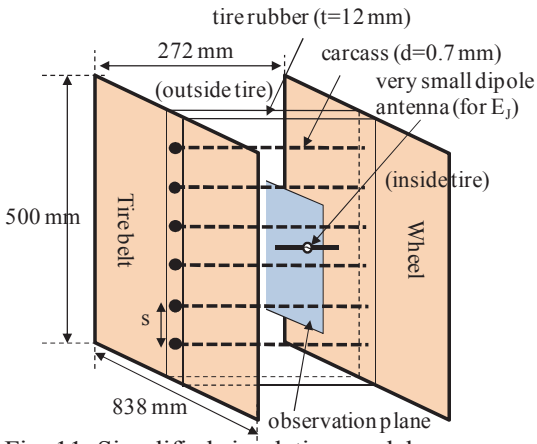

Fig. 11. Simplified simulation model.

Table 1: Electric field distributions in the observation plane

		Electric intensity distribution (dBV/m)	Computation costs
FEM (HFSS)	Without rubber	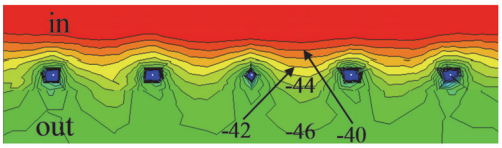	memory: 3.5 GB time: 1631 sec element size of air space between carcasses : λ/75
	With rubber (thickness= 12 mm, ε_r = 10.91 tanδ = 0.14)	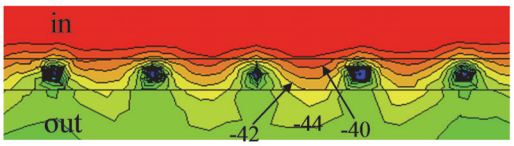	memory: 3.3 GB time: 1634 sec element size of rubber : λ/75
FEM (FEKO)	With rubber (thickness=12 mm, ε_r = 10.91 tanδ = 0.14)	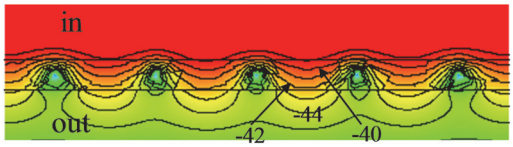	memory: 6.8 GB time: 18,889 sec element size of rubber : λ/75
MoM (FEKO)	rubber mesh size : λ/25	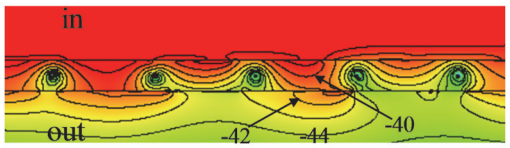	memory: 0.2 GB time: 4481 sec unknown: 4240 cell number: 2000
	rubber mesh size : λ/50	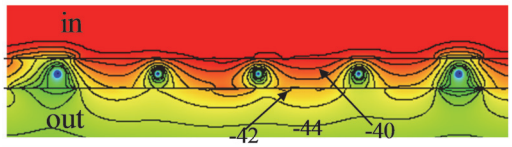	memory: 1.5 GB time: 7868 sec unknown: 10,079 cell number: 4156
	rubber mesh size : λ/75	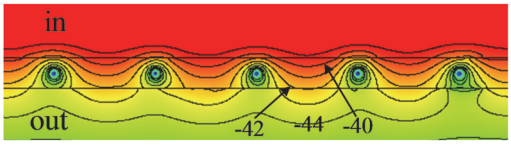	memory: 5.0 GB time: 16,696 sec unknown: 18,374 cell number: 6999

considered adequate. In the case where rubber was retained, electric field penetrations into the carcass wires seem to be enhanced. The electric field intensities at the outside increase by about 1 dB compared to their counterparts when rubber was removed. As a reference, the FEM result by FEKO is also obtained. Almost the same result to HFSS is achieved. On the basis of good agreement of FEM results by HFSS and FEKO, it is concluded that the FEM simulations are correct.

To assess the calculation accuracy of MoM, mesh sizes of the dielectric plate (tire rubber) are changed. In the FEKO simulation, the surface equivalent principle (SEP) algorithm is applied to dielectric plate calculations. In the case of mesh size λ/25, irregular electric field distributions are observed. For mesh size λ/75, almost regular electric field distributions are achieved. Data on electric field intensities are in good agreement with the results of HFSS. Therefore, it is concluded that accurate results can be achieved with a mesh size of λ/75.

V. SIMULATION RESULTS OF AN ACTUAL CARCASS TIRE

A. Fundamental data

As the example of an actual carcass tire, the structure of Fig. 2 is employed. Simulation parameters are summarized in Table 2. The most important parameter is mesh size. In particular, finding out the adequate mesh forms for tire rubbers requires a lot of thought. The result is shown in Fig. 12. Mesh configurations of the tire rubber are matched to the shapes of the spacing of wires. In circumferential directions, three small-sized meshes are used. In radial directions, rather large mesh sizes are selected. In this case, the number of wires used is 36. The wire spacing in the inner and outer rims are 42 and 90 mm, respectively. Observation planes indicated by A and B are oriented perpendicular to the wires.

Mesh sizes of the tire rubber are shown in Table 2. At the inner rim, mesh size λ/67 is selected. The unknown number becomes 17,644. Calculation time of more than 2 hours is needed. In this case, the number of carcass is only 36. In the actual tire, because a large number of carcass wires are used, a more efficient simulation method is required.

Electric field distribution at observation points A and B are shown in Fig. 13. In Fig. 13(a), electric fields outside the tire are suppressed by about 5 dB. In Fig. 13(b), electric field suppressions become 3 dB. In accordance with s increase, suppressions become small. These results are physically appropriate. Therefore, these calculated results are reliable.

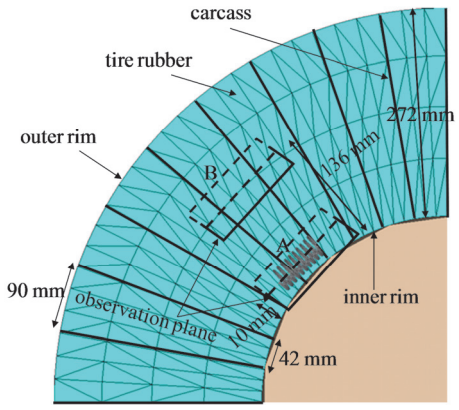

Fig. 12. Mesh configuration of tire rubber.

Table 2: Simulation parameters

CPU clock	Intel® Xeon® CPU 3.00 GHz		
memory	16.0 GB RAM		
simulator	FEKO (MoM)		
Frequency	315 MHz		
mesh sizes	Antenna		λ/600
	wheel	near antenna	λ/100
		other	λ/10
	tire belt		λ/10
	carcass (number, 36)		λ/15
	rubber (SEP method)	radial direction	λ/14
		inner rim	λ/67
		outer rim	λ/32
total mesh number	7,496		
unknown	17,644		
memory usage	2.33 Gbytes		
calculation time	7,571 seconds (2.1 hours)		

B. Electric wave characteristics

Electric field distributions and a radiation characteristic of a carcass tire are calculated. The electric fields inside the tire are shown in Fig. 14. These planes are just 1 mm inside the rubber inner surface. Electric fields with the rubber as shown in Fig. 14(b) become larger compared to those in Fig. 14(a). As for directions of electric field vectors, almost the same directions are achieved in strong field regions. However, small

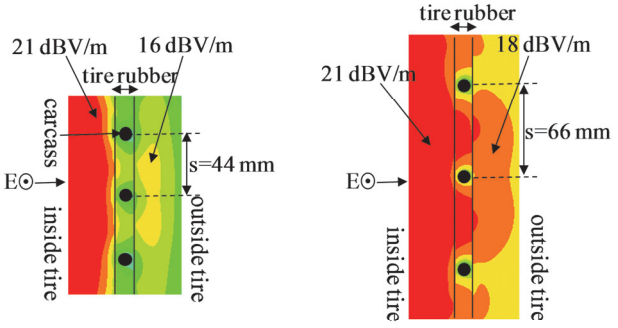

(a) Plane A. (b) Plane B.

Fig. 13. Electric fields at observation planes.

changes of vector directions are produced in weak field regions by the presence of the tire rubber. Next, electric fields in the cross-sectional planes of the tire are shown in Fig. 15. In comparing Fig. 15(a) and (b), the electric fields spilling over to the outside of a tire are increased as a rubber effect. Finally, the radiation power levels of a carcass tire are shown in Fig. 16. The highest levels appear in the side of the tire, reaching a value of -15.6 dBd. This level is 3 dB larger than the result shown in Fig. 9(c). As a conclusion, the presence of rubber increases the electric fields inside a tire and the radiation levels from a tire. By taking into account that a tire rubber is a lossy material, the increase in radiation level is surprising.

VI. Conclusions

The accuracies of the simulation of electric fields in a carcass tire using the MoM scheme of FEKO are determined. The important contributions of this study are as follows:

1) The electric fields inside a tire are compared with those of a coaxial cylindrical resonator chosen as theoretical references.
2) FEM- and MoM-based methods for determining the effect of wires embedded in a dielectric plate are investigated.
3) The adequate mesh sizes of the tire rubber in MoM are determined.
4) Adequate mesh configurations of the tire rubber between carcass wires are developed.
5) By using an actual carcass tire model, the electric fields inside a tire and the characteristics of radiation from a tire are established.

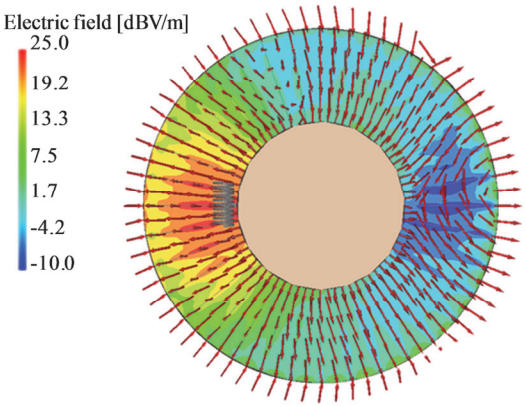

(a) Without rubber.

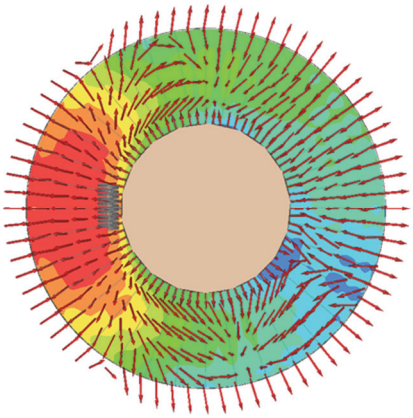

(b) With rubber.

Fig. 14. Electric field distributions inside the tire.

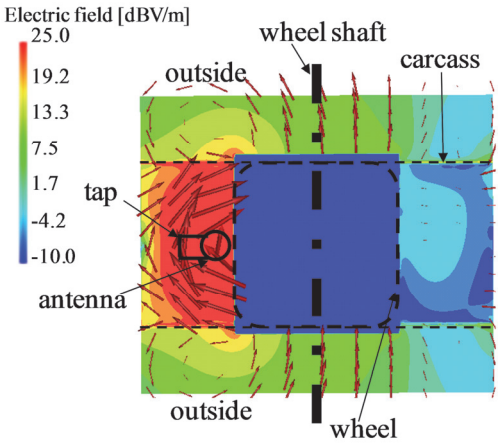

(a) Without rubber.

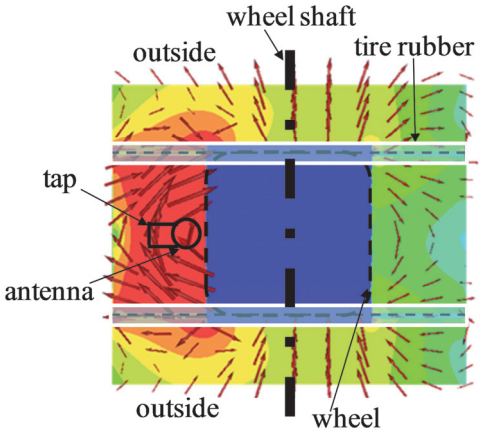

(b) With rubber.

Fig. 15. Electric field distributions in the cross-sectional planes.

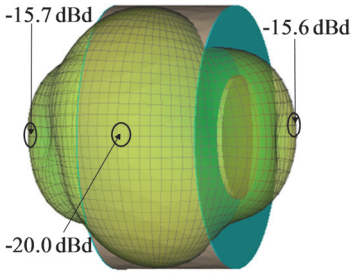

Fig. 16. Radiation pattern.

REFERENCES

[1] http://www.nhtsa.dot.gov/cars/rules/rulings/TPMSfinalrule.6/TPMSfinalrule.6.html

[2] http://www.yrc-pressroom.jp/html/200510717tr001.html

[3] K. Tanoshita, K. Nakatani, and Y. Yamada, "Electric Field Simulations Around a Car of the Tire Pressure Monitoring System," *IEICE Trans. Commun.*, vol. E90-B, no. 9, pp. 2416-2422, 2007.

[4] N. Q. Dinh, N. Michishita, Y. Yamada, and K. Nakatani, "Development of a Very Small Normal Mode Helical Antenna for the Tire Pressure Sensor of TPMS," *ISAP2008*, pp. 186-190, Oct. 2008.

[5] S. D. Walker and D. Chatterjee, "Study of Exact and High-Frequency Code Solvers for Applications to a Conformal Dipole Array," *Applied Computational Electromagnetic Society (ACES) Journal*, vol. 24, no. 6, pp. 550-558, 2009.

[6] N. Q. Dinh, T. Teranishi, N. Michishita, Y. Yamada, and K. Nakatani, "Electromagnetic Simulation Method of a Vehicle Tire Equipped with Carcass," *Applied Computational Electromagnetic Society (ACES) Conference*, session 5, Apr. 2010.